Exact-diagonalization study of the Hubbard model with nearest-neighbor repulsion

Y. Ohta, K. Tsutsui, W. Koshibae, and S. Maekawa
Department of Applied Physics, Nagoya University, Nagoya 464-01, Japan
(Received 2 September 1993; revised manuscript received 5 May 1994)

An exact-diagonalization technique on small clusters is used to study the ground states and single-particle excitations of the Hubbard model with on-site (U) and nearest-neighbor (V) Coulombic repulsive interactions. It is shown that the long-range charge-density-wave state realized in a half-filled two-dimensional square lattice for $4V \gtrsim U$ persists up to quarter filling, and that the doped carriers form a *small* Fermi surface that encloses an area corresponding to the number of doped carriers rather than the total number of electrons involved in the system. The present result offers a well-defined counterexample in the discussion of the Fermi-surface dimensions of strongly correlated electron systems, and may provide a complementary understanding of the *large* Fermi surface believed to exist in the ordinary Hubbard model.

I. INTRODUCTION

Much attention has recently been attracted to the physics of strongly correlated electron systems including high-T_c cuprates, heavy fermions, low-dimensional organic conductors, etc. Long-range Coulomb interaction is known to play a significant role in such systems,[1-4] and much theoretical work has been devoted to clarifying its role. The extended Hubbard model, which takes into account both the on-site and nearest-neighbor replusions, may be the simplest possible model that describes strong electron correlation with long-range Coulomb interaction. The phase diagram of the model at half filling, where either a charge-density-wave (CDW) or a spin-density-wave (SDW) states is realized depending on the interaction strength, has been studied intensively in the context of one-dimensional organic systems.[5-10] A possible relevance of the model to oxide superconductors has also been discussed.[11-14]

In this paper, we will make further investigations of the CDW phase of the extended Hubbard model because, although there are number of published papers, not much is known of its doping dependence and, in particular, low-energy excitation properties. A study of the effects of doping of CDW insulators may provide a complementary understanding of the doping effects in antiferromagnetic insulators, an issue raised by the discovery of cuprate superconductivity.

The single-band extended Hubbard Hamiltonian is written

$$H=-t\sum_{\langle ij\rangle\sigma}(c_{i\sigma}^{\dagger}c_{j\sigma}+\text{H.c.})+U\sum_{i}n_{i\uparrow}n_{i\downarrow}+V\sum_{\langle ij\rangle}n_i n_j \tag{1}$$

with the standard notation, where $c_{i\sigma}^{\dagger}$ creates an electron with spin $\sigma(\uparrow$ and $\downarrow)$ at site i, $n_{i\sigma}=c_{i\sigma}^{\dagger}c_{i\sigma}$ is the number operator, and $n_i=n_{i\uparrow}+n_{i\downarrow}$. $\langle ij\rangle$ represents a nearest-neighbor pair. The parameters t, U, and V are the nearest-neighbor hopping, on-site repulsion, and nearest-neighbor repulsion, respectively. We confine ourselves to low-dimensional systems at $T=0$ K: two-dimensional (2D) systems are mainly examined but some results for one-dimensional (1D) systems are also given as a reference.

We adopt a numerical approach, i.e., the exact diagonalization of finite-size clusters by the Lanczos method, which is known to be a powerful technique to obtain not only the ground states but also dynamical quantities such as single-particle excitation spectra. We take square lattices of the size $\sqrt{8}\times\sqrt{8}$, $\sqrt{10}\times\sqrt{10}$, and 4×4 in 2D, and chains of up to 16 sites in 1D. Periodic boundary conditions are used. The translational and **k**-group symmetries are fully taken into account.[15]

We will show, for the extended Hubbard model in 2D, that the CDW long-range order persists up to quarter filling when the nearest-neighbor repulsion is sufficiently large. This is in contrast to the ordinary half-filled Hubbard model where the antiferromagnetic long-range order collapses very rapidly on doping. We will then show that, in this CDW phase, the Fermi surface is *small* in the sense that it encloses an area proportional to the number of doped holes rather than to the total number of electrons involved in the system. The calculated quasiparticle dispersion suggests that holes introduced into the CDW state propagate freely to second- and third-neighbor sites by tunneling the first-neighbor barrier, with a reduced effective hopping parameter. The result thus offers a well-defined counterexample in the discussion on the Fermi-surface dimension of the ordinary $V=0$ Hubbard and t-J models where a controversy still exists.[16-18] We will also show that, at quarter filling, a gap opens in the single-particle excitation spectrum, of which the size is given by $\min(U,4V)$ when $t\to0$, and SDW long-range order coexists with the CDW long-range order. The SDW fluctuation exhibits a filling-dependent incommensurate behavior in both 1D and 2D. The present results are compared with our previously obtained results[19] for the ordinary Hubbard model.

This paper is organized as follows. We first present the equal-time charge and spin correlation functions in Sec. II, whereby the doping dependence of the CDW and

SDW long-range orders is examined. Then, in Sec. III, we present the single-particle excitation spectra and momentum distribution functions, and discuss the low-energy excitations and Fermi surface of the model. A summary of this paper with a schematic phase diagram of the model is given in Sec. IV. Some of our preliminary results have been published in Ref. 20.

II. GROUND STATE

Let us first examine the ground state. We measure correlation functions for zero-momentum ground states (unless otherwise stated), as has always been done in the standard finite-size calculations of physical quantities. This is well justified because in order for the finite-cluster ground state to be "representative" for the ground state in the thermodynamic limit it should have the same quantum numbers, i.e., vanishing total momentum. We define the equal-time charge correlation function as

$$C(\mathbf{q})=\frac{1}{N}\sum_{ij}\langle n_i n_j\rangle e^{i\mathbf{q}\cdot(\mathbf{R}_i-\mathbf{R}_j)}, \tag{2}$$

where $\mathbf{R}_i$ is the lattice vector, N is the number of lattice sites, and $\langle\cdots\rangle$ represents the ground-state expectation value. The calculated results for $C(\mathbf{q})$ at $\mathbf{q}=(\pi,\pi)$ are shown in Fig. 1 as a function of the filling n, where we take $U/t=8$ and $V/t=3$. It is found that the cluster-size dependence of $C(\pi,\pi)/N$ is very small for $0.5\le n\le 1$; it may well remain finite in the thermodynamic limit, indicating a $\sqrt{2}\times\sqrt{2}$ CDW long-range order. The order persists up to quarter filling. The transition into this CDW phase caused by increasing V is associated with a ground-state energy-level crossing in the finite-size calculation. The calculated values of $C(\mathbf{q})$ at momenta other than $\mathbf{q}=(\pi,\pi)$ are small and featureless for any filling. No behaviors suggesting discommensuration are noticed; i.e., the removal of electrons by doping does not influence the CDW wavelength. The motion of holes in the CDW order is discussed in Sec. III. In the parameter region $0<4V\lesssim U$ we expect an enhancement of the charge fluctuation which couples with the lattice degrees of freedom and may lead to a soft-phonon instability.[5,13,14] The results for $C(\pi,\pi)$ in this parameter region, however, indicate that the electronic system alone does not lead to the CDW long-range order.

The equal-time spin correlation function

$$S(\mathbf{q})=\frac{1}{N}\sum_{ij}\langle s_i^z s_j^z\rangle e^{i\mathbf{q}\cdot(\mathbf{R}_i-\mathbf{R}_j)} \tag{3}$$

is also calculated, where s_i^z is the z component of the spin operator at site i. The results are shown in Fig. 2. Approaching quarter filling from half filling, we observe an enhancement of $S(\mathbf{q})$ at $\mathbf{q}=(\pi,0)$, $(\pi/2,\pi/2)$, and $(0,\pi)$, which suggests a SDW ordering at quarter filling. The equivalent value of $S(\mathbf{q})$ at these momenta [see Fig. 2(d)] is due to the hypercubic symmetry of the 4×4 cluster. The strong-coupling perturbation expansion indicates that the spin degrees of freedom of the system at quarter filling are described by a J-J' model, where J and J' are second- and third-nearest-neighbor antiferromagnetic exchange interactions, respectively. We obtain the spin Hamiltonian

$$H=\mathcal{P}\left[J\sum_{\langle ij\rangle}^{\text{2nd}}\mathbf{s}_i\cdot\mathbf{s}_j+J'\sum_{\langle ij\rangle}^{\text{3rd}}\mathbf{s}_i\cdot\mathbf{s}_j\right]\mathcal{P} \tag{4}$$

with

$$J=\frac{4t^4}{9V^2}\left[\frac{4}{U}+\frac{1}{V}+\frac{4}{U+4V}\right] \tag{5}$$

and

$$J'=\frac{4t^4}{9V^2}\left[\frac{1}{U}+\frac{2}{U+4V}\right] \tag{6}$$

to fourth order of t. The summations in the first and second terms of Eq. (4) are over second-neighbor and third-neighbor pairs, respectively, and $\mathcal{P}$ represents the projection to the states where the electrons are only in

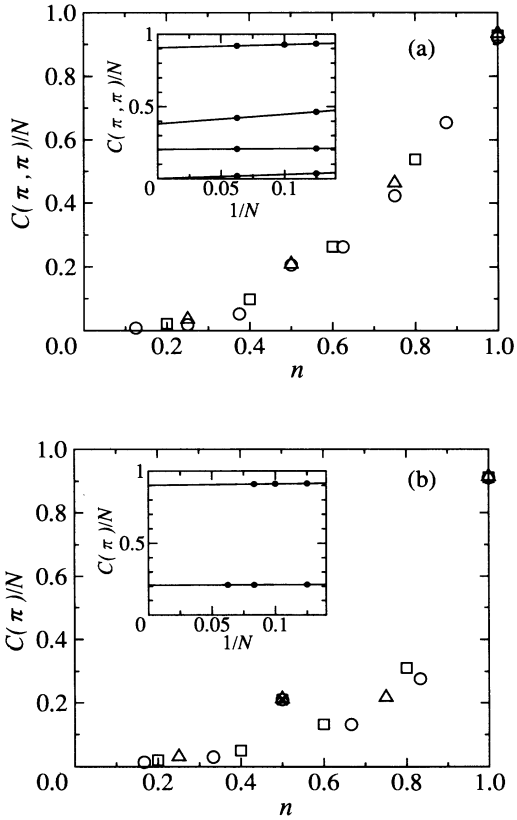

FIG. 1. Filling dependence of the charge correlation function in (a) 2D and (b) 1D extended Hubbard clusters. (a) shows $C(\mathbf{q})/N$ at $\mathbf{q}=(\pi,\pi)$ calculated for the $\sqrt{8}\times\sqrt{8}(\Delta)$, $\sqrt{10}\times\sqrt{10}(\square)$, and $4\times4(\circ)$ clusters with $U/t=8$ and $V/t=3$. (b) shows $C(q)/N$ at $q=\pi$ calculated for the 8-site ($\triangle$), 10-site ($\square$), 12-site ($\circ$), and 16-site ($\times$) rings with $U/t=12$ and $V/t=7$. Insets show the size-scaling behaviors of available data; the lines, from the top, show the data at $n=1$, 0.75, 0.5, and 0.25 in (a), and $n=1$ and 0.5 in (b).

one sublattice and there are no doubly occupied sites. The relation $J' \lesssim J/3$ holds for any values of U and V that sustain the CDW order, so that the frustration[21] of the exchange interactions is rather small. It is thus expected that the 2×2 SDW long-range order, which corresponds to the divergence of $S(\mathbf{q})$ at $\mathbf{q}=(\pi/2,\pi/2)$, appears in the thermodynamic limit. An incommensurate peak is observed in the spin correlation function at around $0.5 < n \lesssim 0.75$ in 2D, which is due to strong frustration caused by extra spins introduced into the SDW order at quarter filling.

The CDW plus SDW long-range order at quarter filling may persist even when $4V < U$, because the system remains insulating as discussed below. Since the ordinary $V=0$ Hubbard model shows no indications of long-range order at this filling, a phase transition is expected when a finite V term is present. Further studies are required to clarify what is the critical value of V/t and whether any experiments can provide this situation. A quantum Monte Carlo study of this problem is now in progress.

The charge and spin correlation functions in 1D systems are also calculated. We examine the case where the interaction strengths are sufficiently large, i.e., $U/t=12$ and $V/t=7$. The results are shown in Figs. 1(b) and 3. The behavior looks similar to the 2D systems. (i) $C(q)/N$ at $q=\pi$ is almost size independent at $n=1$ and $\frac{1}{2}$, but at

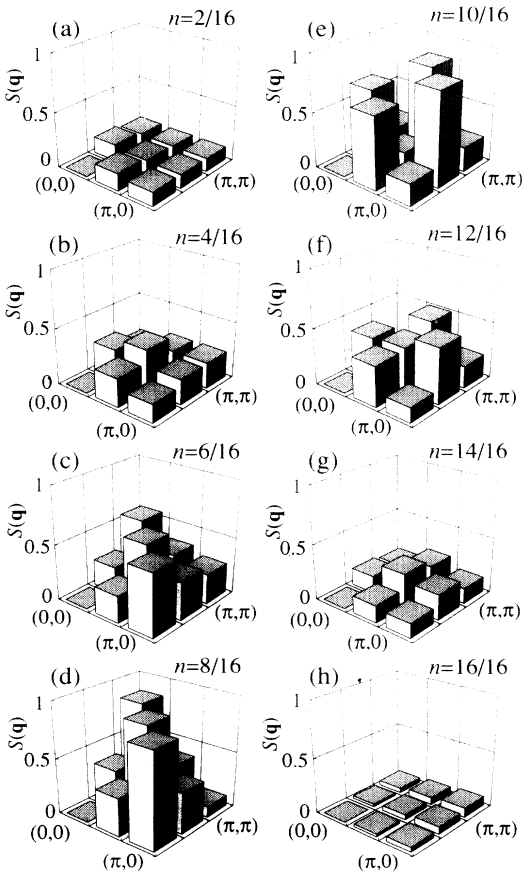

FIG. 2. Filling dependence of the spin correlation function $S(\mathbf{q})$ calculated for the 4×4 cluster with $U/t=8$ and $V/t=3$. The height of the square bar at each $\mathbf{q}$ point indicates the values of $S(\mathbf{q})$. The part of the Brillouin zone with $q_x \geq 0$ and $q_y \geq 0$ is shown.

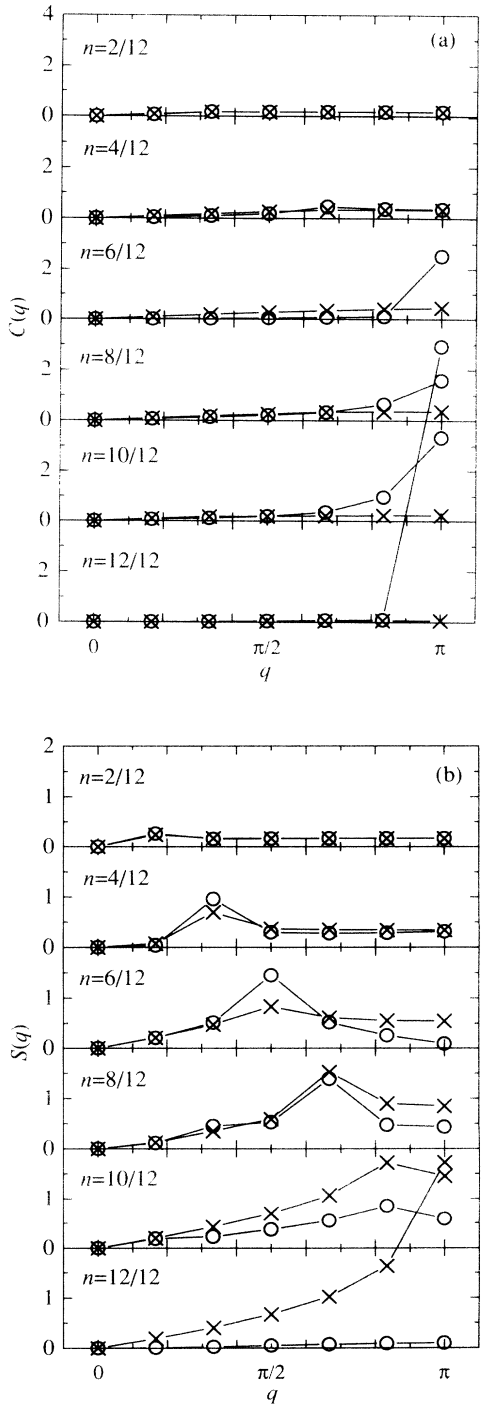

FIG. 3. Filling dependence of (a) charge and (b) spin correlation functions calculated for the 1D 12-site ring with $U/t=12$ and $V/t=7$ ($\circ$), and with $U/t=12$ and $V/t=0$ ($\times$).

fillings inbetween it decreases significantly with N. CDW long-range order is then suggested at least at $n=1$ and $\frac{1}{2}$. The momentum dependence of $C(q)$ suggests no discommensurate behaviors in the CDW phase, as in the 2D case. (ii) The peak in $S(q)$ at $q=2k_F$, which indicates an incommensurate SDW fluctuation, is observed clearly in a wide region of n around quarter filling. This incommensurability comes from the Fermi-surface nesting and is enhanced with increasing U.

III. SINGLE-PARTICLE EXCITATION

Now let us examine the single-particle excitations in the extended Hubbard model. First, we show the schematic density of states at $4V>U\gg t$ in 2D (see Fig. 4), which enables one to get a rough idea of the evolution of the spectral functions upon doping. At half filling, a gap of the size $8V-U$ opens up between lower and upper bands, since doubly occupied and empty sites are arranged regularly to form the $\sqrt{2}\times\sqrt{2}$ CDW configuration. By removing an electron from the half-filled system, the spectral weight of 1 appears at the top of the lower band. The Fermi energy lies at this energy, so that the system is metallic. The same weight also appears at zero energy. Spectral-weight transfer to this type continues until quarter filling. Note that this is in contrast to the ordinary Hubbard model where the weight of 2 appears at the top of the lower band. At quarter filling, there appears a gap again, the size of which scales with U for $4V>U$. This gap does not even vanish for $4V<U$ and has the size of $4V$ at $t\to 0$ although it may close to vanishing if t is too large compared with V. The realization of the quarter-filled insulator, which is a kind of Wigner lattice, seems to be an interesting experimental problem.[22,23] By removing an electron from the quarter-filled insulator, the spectral weight of 2 appears at the top of the band around zero energy, and the system again becomes metallic. The Fermi energy goes through this band on further doping. The finite-size cluster calculations properly reproduce such an evolution of the spectral function.

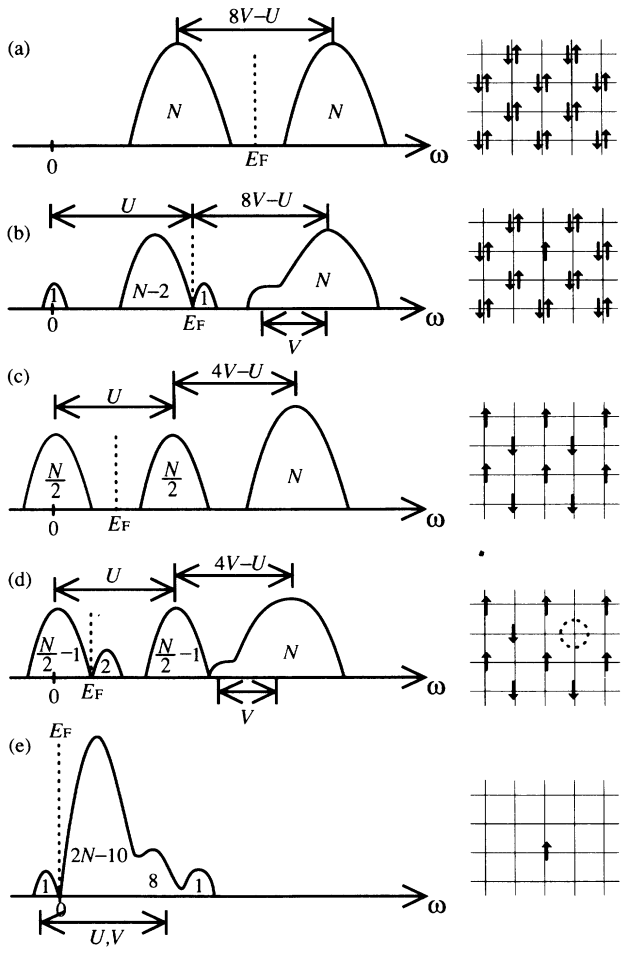

FIG. 4. Schematic representation of the density of states in the extended Hubbard model in 2D. The numbers indicate spectral weight in the N-site lattice. The parameter range of $4V>U\gg t$ is assumed. Illustrated are (a) the state at half filling, (b) the state where an electron is removed from half filling, (c) the state at quarter filling, (d) the state where an electron is removed from quarter filling, and (e) the one-electron state in an otherwise empty lattice. The corresponding electron configurations are also shown.

A possible quasiparticle picture may be extracted from the single-particle spectral function $A(\mathbf{k},\omega)$, which is defined as the sum

$$A(\mathbf{k},\omega)=A^{-}(\mathbf{k},-\omega)+A^{+}(\mathbf{k},\omega) \tag{7}$$

of the photoemission (PES)

$$A^{-}(\mathbf{k},\omega)=\sum_{\nu\sigma}|\langle\psi_\nu^{L-1}|c_{\mathbf{k}\sigma}|\psi_0^L\rangle|^2\delta(\omega-E_\nu^{L-1}+E_0^L) \tag{8}$$

and inverse photoemission (IPES)

$$A^{+}(\mathbf{k},\omega)=\sum_{\nu\sigma}|\langle\psi_\nu^{L+1}|c_{\mathbf{k}\sigma}^{\dagger}|\psi_0^L\rangle|^2\delta(\omega-E_\nu^{L+1}+E_0^L) \tag{9}$$

spectra. E_ν^L and ψ_ν^L are the νth excited eigenvalue and eigenvector of the L-electron system, respectively, where $\nu=0$ denotes the ground state, and $c_{\mathbf{k}}^{\dagger}$ is the Fourier transform of the creation operator $c_{i\sigma}^{\dagger}$. The Lanczos algorithm is used via the continued-fraction expansion of Eqs. (8) and (9). By adding a small imaginary number $i\eta$ to ω, we give a Lorentzian smoothing to the spectra, which otherwise consist of a set of δ functions. The value $\eta=0.15t$ is used.

First let us examine the spectral function at half filling. The ground state is at $\mathbf{k}=(0,0)$ with the point-group symmetry A_1. The result for $A(\mathbf{k},\omega)$ is shown in Fig. 5(a). We find that there appear lower and upper bands, which are separated by a gap. The spectra are represented almost entirely by dispersive low-energy states, forming a quasiparticle band. The dispersion of the quasiparticle is represented very well by the following expression obtained from the second-order perturbation expansion:

$$\varepsilon_{\mathbf{k}}=-4t_{\text{eff}}^{(2)}\cos k_x\cos k_y -2t_{\text{eff}}^{(3)}(\cos 2k_x+\cos 2k_y)+\text{const} \tag{10}$$

with the effective second- and third-neighbor hopping

strengths of

$$t_{\text{eff}}^{(2)} = 2t_{\text{eff}}^{(3)} = \frac{2t^2}{6V-U} \ . \tag{11}$$

An intuitive picture obtained from this result is that the single hole introduced into the CDW state propagates freely to a second- or third-neighbor site by tunneling the first-neighbor barrier, with the effective hopping strengths of $t_{\text{eff}}^{(2)}$ or $t_{\text{eff}}^{(3)}$, respectively. Such a structure of the single-hole spectral function is in strong contrast to the ordinary Hubbard and t-J model calculations[19] where a broad band of the incoherent continua is observed beside the quasiparticle peak at the edge of the gap. The hole propagation in the CDW state is not associated with spin distortions, which play an essential role in the SDW state.

Next let us examine the filling dependence of the spectral function (see Figs. 5–7). In the case of two holes (or at $n=\frac{14}{16}$) the ground state has the momentum $\mathbf{k}=(0,0)$ with the A_1 point-group symmetry [which is degenerate with the $\mathbf{k}=(\pi,\pi)$ state with the B_2 point-group symmetry]. The spectral function is calculated for the zero-momentum ground state and is shown in Fig. 5(b). As in the standard Hubbard-model cases,[19] we find that, upon doping the half-filled insulator, the Fermi level is shifted to the top of the lower band, and these appears spectral weight just above the Fermi energy mainly at $\mathbf{k}=(\pi,0)$, a gap remaining to the deformed upper band. However, in contrast to the Hubbard-model results,[19] no low-energy spectral weights appear at $\mathbf{k}=(\pi,\pi)$ and $(\pi,\pi/2)$, so that the dispersion of the low-energy quasiparticle states remains basically unchanged. Two holes mainly occupy the momentum $(\pi,0)$ which is identical to $(0,\pi)$ in the "antiferromagnetic" Brillouin zone. The rigid-band picture thus works well in this system; the hole-pocket-like Fermi surface is realized, which encloses an area corresponding to the number of doped holes rather than to the total number of electrons in the system. The position of the hole pocket is determined by the interaction of two holes in the ground state: the two holes are mainly located at $\mathbf{k}=(\pi,0)$ [or at $\mathbf{k}=(0,\pi)$] and form a zero-

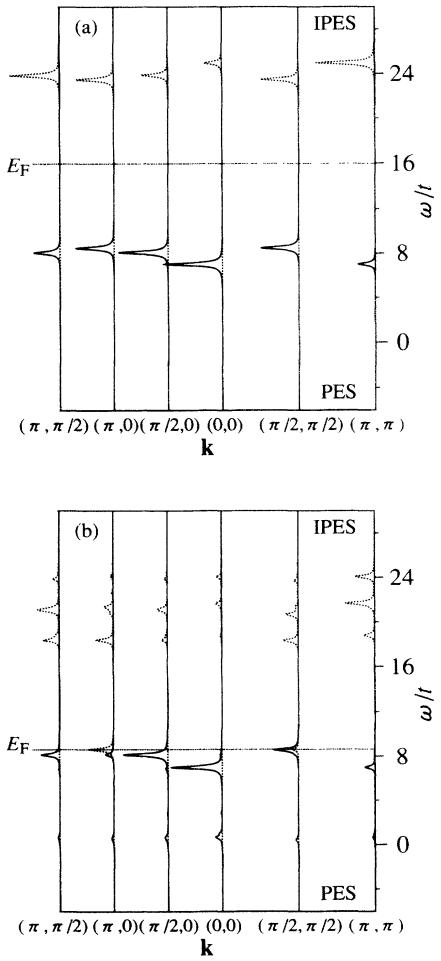

FIG. 5. Single-particle excitation spectra $A(\mathbf{k},\omega)$ at (a) half filling ($n=1$) and (b) 12.5% hole doping ($n=0.875$) calculated for the 4×4 cluster with $U/t=8$ and $V/t=3$.

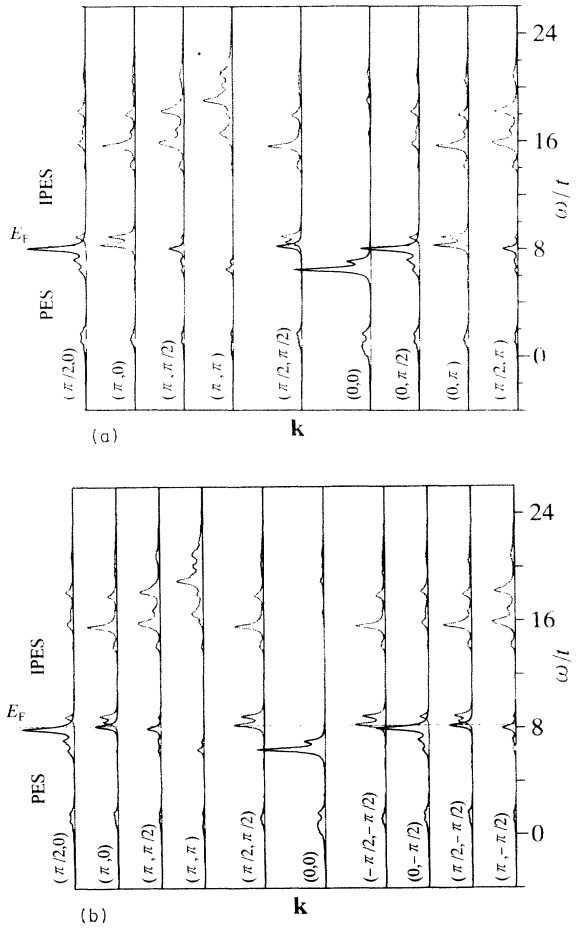

FIG. 6. Single-particle excitation spectra $A(\mathbf{k},\omega)$ at 25% hole doping ($n=0.75$) calculated for the 4×4 cluster with $U/t=8$ and $V/t=3$. In (a) the ground state with momentum $(\pi,0)$ is used, and in (b) that with $(\pi/2,\pi/2)$ is used. The results include all the inequivalent k points in the Brillouin zone.

momentum pair in agreement with the ground-state momentum $\mathbf{k}=(0,0)$, which explains the position of the hole pocket observed in the spectral function. The ground state with $\mathbf{k}=(\pi,\pi)$, on the other hand, involves two holes that are located at $\mathbf{k}=(\pi/2,\pi/2)$ [and at $(-\pi/2,-\pi/2)$ which is equivalent to $(\pi/2,\pi/2)$ in the "antiferromagnetic" Brillouin zone] and form a finite-momentum pair. Thus the calculated spectral function for the ground state with $\mathbf{k}=(\pi,\pi)$ also shows the hole-pocket-like Fermi surface at momenta $\mathbf{k}=(\pi/2,\pi/2)$ [or

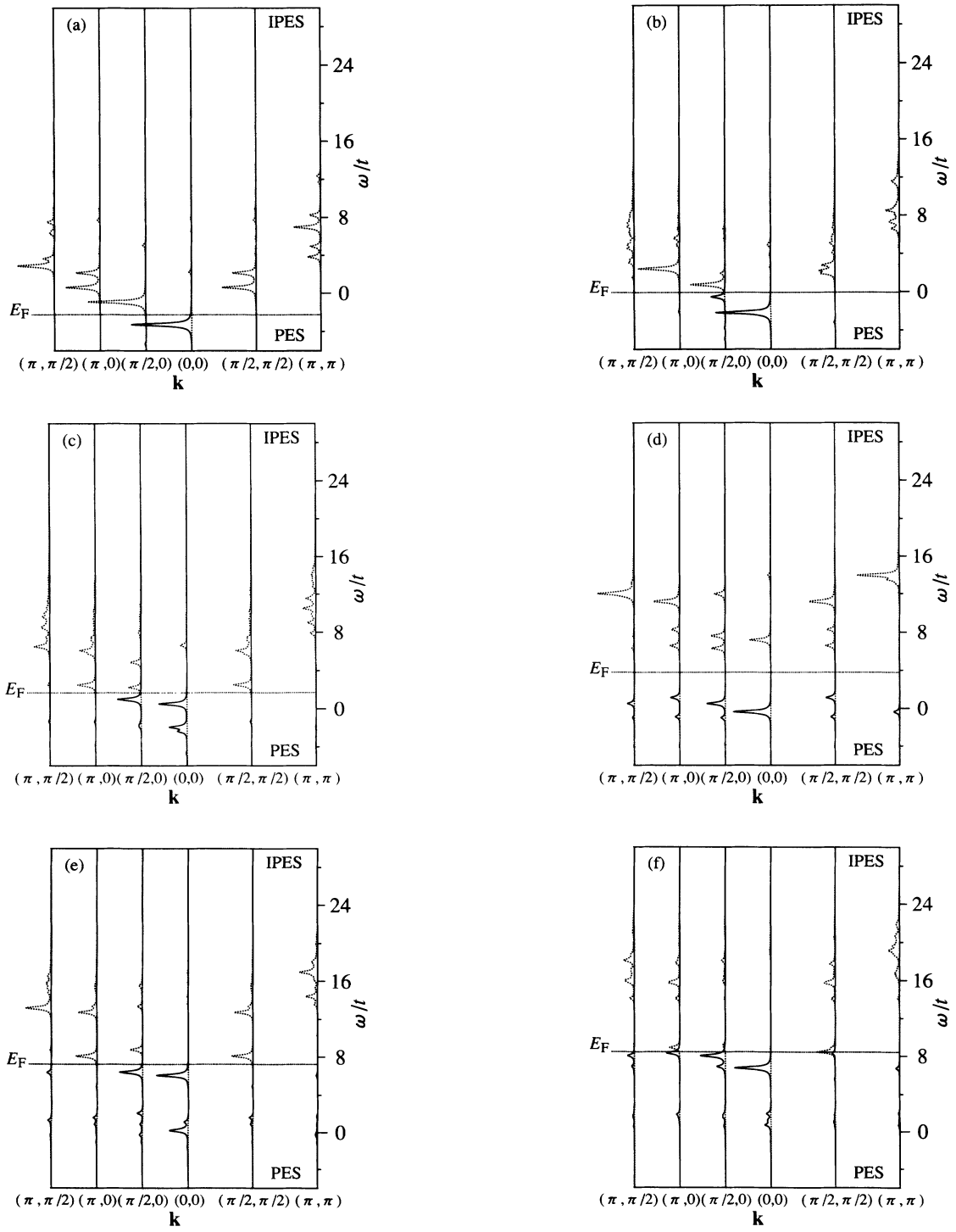

FIG. 7. Single-particle excitation spectra $A(\mathbf{k},\omega)$ at various fillings (except near half filling) calculated for the 4×4 cluster with $U/t=8$ and $V/t=3$. Displayed are the spectra at (a) $n=\frac{2}{16}$, (b) $n=\frac{4}{16}$, (c) $n=\frac{6}{16}$, (d) $n=\frac{8}{16}$, (e) $n=\frac{10}{16}$, and (f) $n=\frac{12}{16}$.

$(-\pi/2,-\pi/2)$]. Thus, independently of the ground-state momentum, a *small* Fermi surface enclosing an area corresponding to the number of doped holes is realized; the position is determined by the interaction between holes and is located at the momenta $\mathbf{k}=(\pi,0)$ [or $(\pi/2,\pi/2)$] in the 4×4 cluster.

In the case of four holes (or at $n=\frac{12}{16}$) the ground state has the momentum $\mathbf{k}=(\pi,0)$ or $(\pi/2,\pi/2)$: the energy of the state is slightly lower (by $0.0854t$ in the case of $U/t=8$ and $V/t=3$) than the energy of the $\mathbf{k}=(0,0)$ ground state. Such nonzero ground-state momenta can be understood because, due to their weak interactions, one hole is located at $\mathbf{k}=(\pi,0)$ [or at $\mathbf{k}=(\pi/2,\pi/2)$], and the other three holes are located with zero total momentum at, e.g., $\mathbf{k}=(0,\pi)$, $(\pi/2,-\pi/2)$, and $(-\pi/2,-\pi/2)$, i.e., at the edge of the "antiferromagnetic" Brillouin zone. Note that, because momenta of such mobile holes determine the ground-state momentum, the choice of nonzero-momentum ground-state does not affect the CDW long-range order (discussed in Sec. II) of "background" electrons. The single-particle spectral functions calculated for these nonzero-momentum ground states are shown in Fig. 6. We find that, in agreement with the above picture, the low-energy quasiparticle peaks appear at $\mathbf{k}=(\pi,0)$, $(0,\pi)$, and $(\pi/2,\pi/2)$ for the $(\pi,0)$ ground state, and at $\mathbf{k}=(\pi/2,\pi/2)$, $(-\pi/2,-\pi/2)$, $(\pi,0)$, and $(\pi/2,-\pi/2)$ for the $(\pi/2,\pi/2)$ ground state. No low-energy peaks appear at $\mathbf{k}=(\pi,\pi)$ and peaks of very little weight appear at $\mathbf{k}=(\pi,\pm\pi/2)$ and $(\pm\pi/2,\pi)$. The rigid-band picture thus works well also in the four-hole case; the dispersion of the low-energy quasiparticle states observed at half filling remains basically unchanged. The area of the hole Fermi surface is now rather extended to include four holes; for the $(\pi,0)$ ground state, it includes $\mathbf{k}=(\pi,0)$ and $(0,\pi)$ and partially includes $\mathbf{k}(\pm\pi/2,\pm\pi/2)$, and for the $(\pi/2,\pi/2)$ ground state, it includes $\mathbf{k}=(\pi/2,\pi/2)$ and $(-\pi/2,-\pi/2)$ and partially includes $\mathbf{k}=(\pi,0)$, $(0,\pi)$, $(\pi/2,-\pi/2)$, and $(-\pi/2,\pi/2)$. However, when one uses a ground state of finite-size clusters to represent the ground state of the thermodynamic limit, one should use the state with the same quantum numbers as that expected in the thermodynamic limit, i.e., the state with vanishing total momentum. We calculate the single-particle spectral functions for this zero-momentum ground state, and we show the results in Fig. 7(f). We again find the same indications of the validity of the rigid-band picture. The situation holds also in the six-hole case [see Fig. 7(e)]. In the eight-hole case, i.e., at quarter filling, we find a gap in the spectral function as discussed above and the system becomes insulating [see Fig. 7(d)]. Thus, between half and quarter fillings, a *small* Fermi surface, which encloses an area corresponding to the number of doped holes rather than to the total number of electrons in the system, is realized. Such a *small* Fermi surface is not surprising because the CDW long-range order may persist between half and quarter fillings as discussed in Sec. II. An intuitive picture in real space would be that, on doping, doubly occupied sites become singly occupied without disturbing the CDW order and holes in the singly occupied sites are mobilized to be natural carriers.

The calculated momentum distribution function

$$n(\mathbf{k})=\sum_{\sigma}\langle c^{\dagger}_{\mathbf{k}\sigma}c_{\mathbf{k}\sigma}\rangle \tag{12}$$

is consistent with the above picture. Results of the 4×4 cluster calculation are shown in Fig. 8. One should first of all note that the overall momentum dependence in $n(\mathbf{k})$ simply stems from the nearest-neighbor-hopping kinetic-energy term of the Hamiltonian, and has nothing to do with the shape of the Fermi surface.[18] However, in agreement with the calculated single-particle spectral functions, we find characteristic dips at some k points in the calculated momentum distribution function. The dips appear, e.g., at $\mathbf{k}=(\pi,0)$ and $(0,\pi)$ for $n=\frac{14}{16}$ and at $\mathbf{k}=(\pi/2,\pi/2)$ for $n=\frac{12}{16}$ [see Figs. 8(f) and 8(g)] where the low-energy peaks appear in the inverse photoemission spectra. This dip structure of $n(\mathbf{k})$ indicates that the two holes (or four holes) introduced into the half-filled CDW state predominantly occupy those momentum rather than momenta outside the Fermi surface of corresponding

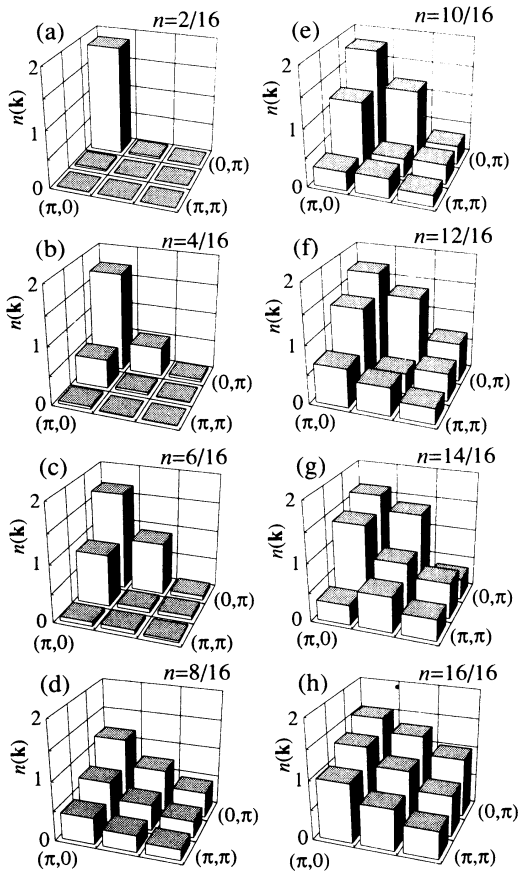

FIG. 8. Momentum distribution function $n(\mathbf{k})$ in the 2D extended Hubbard model calculated for the 4×4 cluster with $U/t=8$ and $V/t=3$. Height of the square bar at each $\mathbf{k}$ point indicates the value of $n(\mathbf{k})$. The part of the Brillouin zone with $q_x\geq0$ and $q_y\geq0$ is shown.

noninteracting systems. Such a structure can be noticed even for $n=\frac{10}{16}$ [see Fig. 8(e)], and also for the nonzero-momentum ground states calculated at $n=\frac{12}{16}$. Although the shape of the Fermi surface realized in the thermodynamic limit is still difficult to predict, a simple expectation consistent with the calculated momentum distributions and single-particle excitation spectra would be that at very low doping levels it appears somewhere along the edge of the "antiferromagnetic" Brillouin zone, i.e., the line connecting $(\pi,0)$, $(\pi/2,\pi/2)$ and $(0,\pi)$, and on further doping it extends to form a Fermi surface of a canal-like shape which includes those k points.

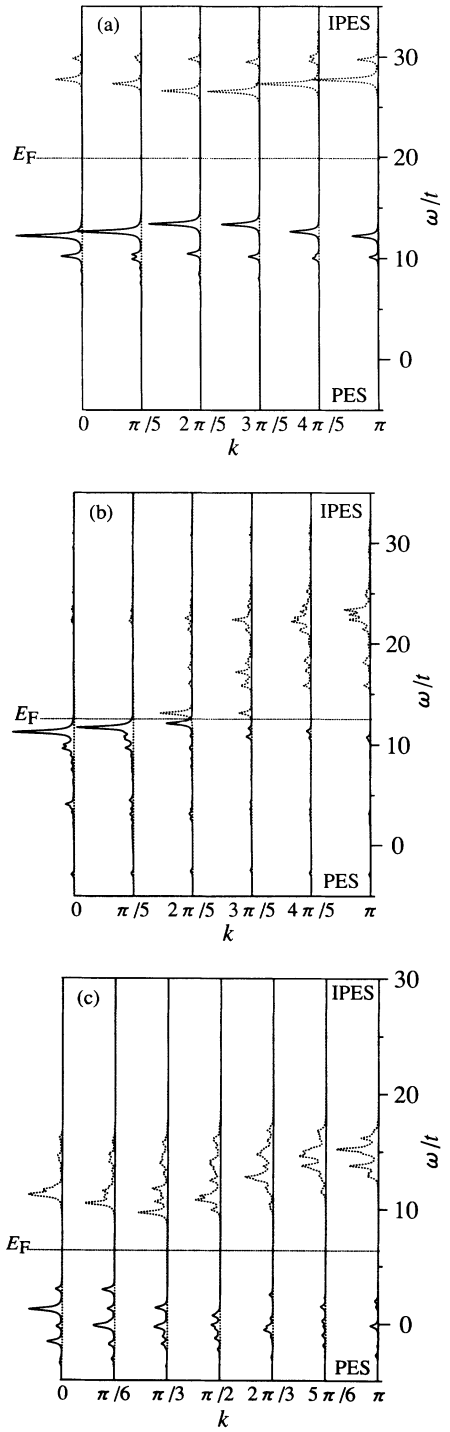

FIG. 9. Single-particle excitation spectra $A(k,\omega)$ in the 1D extended Hubbard model calculated with $U/t=12$ and $V/t=7$ for (a) the 10-site ring at $n=1$, (b) the 10-site ring at $n=0.8$, and (c) the 12-site ring at $n=0.5$.

It should be noted that we are discussing the Fermi surface within a finite-size calculation with no broken symmetry, demonstrating that a number of indications of a small Fermi surface are observed. This is not surprising because the size of the clusters (l) is smaller than the correlation length of the charge ordering, and the velocity of the quasiparticles (v) is faster than the corresponding charge fluctuations in the clusters, so that the energy scale (ϵ) of the present finite-size calculations is sufficiently low, i.e., $l/v \ll 1/\epsilon$, to detect the small-Fermi-surface indications. A possible caution would then be that there can be no *long-range* CDW order in the limit of infinite spatial scale, and thus the true Fermi surface defined in the zero-energy limit is large as expected from Luttinger's theorem.[24] In the present case, however, the size-scaling behavior of the calculated charge correlation function [see Fig. 1(a)] suggests the realization of long-range CDW order in the thermodynamic limit; we therefore expect that the observed small-Fermi-surface indications will survive even in the zero-energy excitation limit of the infinite system. The present calculations would rather provide a well-defined example by which we know how the single-particle spectra and momentum distributions behave in the finite-size calculations in a situation where a small Fermi surface is realized.

The single-particle spectral function at quarter filling is shown in Fig. 7(d). We find a gap, at the edge of which we again observe the dispersive state. An indirect gap is observed in the results of the 4×4 cluster. On further doping we find that the spectral function seems to approach the picture expected for noninteracting electrons (see Fig. 7).

The doping-induced changes in the calculated single-particle spectra in 1D systems are similar to the 2D case as shown in Fig. 9, although further studies are required to show the presence of CDW long-range order (see Sec. II) and to say anything about the Fermi surface.

IV. SUMMARY

We have studied the extended Hubbard model in low dimensions by calculating the charge and spin correlation functions, single-particle excitation spectra, and momentum distribution functions via the exact-diagonalization technique for small clusters. The schematic phase diagram in the 2D square lattice, which is extracted from these calculations, is shown in Fig. 10.

It has been argued that the model at $T=0$ K exhibits a unique ordered phase in the thermodynamic limit, which is characteristic of the following. (i) $\sqrt{2}\times\sqrt{2}$ CDW long-range order is realized at half filling when $4V \gtrsim U$, and persists up to quarter filling. (ii) 2×2 SDW order coexists with the CDW order at quarter filling, the spin degrees of freedom being described by a J-J' model. The

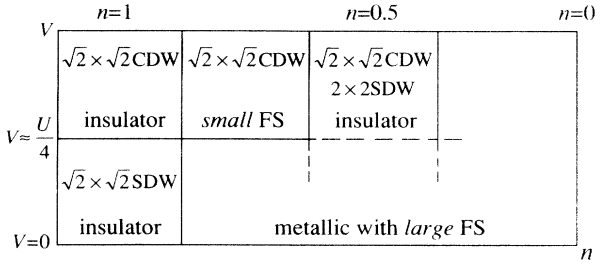

FIG. 10. Schematic phase diagram of the 2D extended Hubbard model. FS means Fermi surface.

single-particle excitations show a gap at this filling, which scales with $\min(U,4V)$ at $t\to 0$. (iii) An incommensurate peak is observed in the spin correlation function for $0.5<n\lesssim 0.75$ in 2D and in a wide region around quarter filling in 1D. The charge correlation function shows no appreciable incommensurate peaks in either 1D or 2D. (iv) The single-particle spectral weight above the Fermi level transferred due to doping the half-filled CDW phase increases as $\alpha\delta$ with $\alpha\simeq 1$ where δ is the doping rate, which is in contrast to $\alpha\simeq 2$ in the SDW phase of the ordinary Hubbard model. Doping of the quarter-filled insulating phase gives a transfer of $\alpha\simeq 2$. (v) The calculated single-particle excitations spectra in 2D indicate that the holes introduced into the CDW phase propagate to second- or third-neighbor sites by tunneling the first-neighbor barrier with a reduced effective hopping strength. The doping dependence of the spectral functions (up to quarter filling) indicates the validity of the rigid-band picture in this system. The interaction between holes is not significant except for the strong on-site repulsion. (vi) The calculated momentum distribution functions indicate that, on doping the half-filled CDW phase, the characteristic dips in $n(\mathbf{k})$ appear at momenta $\mathbf{k}=(\pi,0)$, $(\pi/2,\pi/2)$, and their equivalent points. (vii) The results (v) and (vi) indicates that the quasiparticle Fermi surface emerging on doping is small in the sense that it encloses the area of the number of doped holes rather than the area corresponding to the total number of electrons involved in the system. The shape of the small Fermi surface realized in the thermodynamic limit is still difficult to predict, but the simplest expectation would be that at very low dopings it appears somewhere along the line connecting $(\pi,0)$, $(\pi/2,\pi/2)$, and $(0,\pi)$, and on further doping it extends to form a canal-like Fermi surface including these k points. The present result offers a well-defined counterexample in the discussion of the Fermi-surface dimensions of strongly correlated electron systems, and may provide a complementary understanding of the large Fermi surface believed to exist in the ordinary Hubbard model.

ACKNOWLEDGMENTS

We would like to thank Professor A. Fujimori and Dr. R. Eder for valuable discussions. This work was supported by Grants-in-Aid for Scientific Research on Priority Areas "Mechanism of Superconductivity" and "Computational Physics as a New Frontier in Condensed Matter Research" from the Ministry of Education, Science, and Culture of Japan. Computations were partly carried out in the Computer Center of the Institute of Molecular Science, Okazaki National Research Institutes.

[1]J. B. Torrance, J. E. Vazquez, J. J. Mayerle, and V. Y. Lee, Phys. Rev. Lett. **46**, 253 (1981).
[2]C. M. Varma, S. Schmitt-Rink, and E. Abrahams, Solid State Commun. **62**, 681 (1987).
[3]Y. Ohta, T. Tohyama, and S. Maekawa, Phys. Rev. Lett. **66**, 1228 (1991); Phys. Rev. B **43**, 2968 (1991).
[4]T. Kasuya, Y. Haga, Y. S. Kwon, and T. Suzuki, Physica B **186-188**, 9 (1993).
[5]J. E. Hirsch and D. J. Scalapino, Phys. Rev. B **27**, 7169 (1983); **29**, 5554 (1984).
[6]J. E. Hirsch, Phys. Rev. Lett. **53**, 2327 (1984); Phys. Rev. B **31**, 6022 (1985).
[7]B. Fourcade and G. Spronken, Phys. Rev. B **29**, 5089 (1984); **29**, 5096 (1984).
[8]J. W. Cannon and E. Fradkin, Phys. Rev. B **41**, 9435 (1990); J. W. Cannon, R. T. Scalettar, and E. Fradkin, *ibid.* **44**, 5995 (1991).
[9]T. Nishino, J. Phys. Soc. Jpn. **61**, 3651 (1992).
[10]Y. Zhang and J. Callaway, Phys. Rev. B **39**, 9397 (1989).
[11]J. Callaway, D. P. Chen, D. G. Kanhere, and Q. Li, Phys. Rev. B **42**, 465 (1990).
[12]Y. Mizuno and H. Namaizawa, Prog. Theor. Phys. **80**, 353 (1988).
[13]J. Zhong and H.-B. Schüttler, Phys. Rev. Lett. **69**, 1600 (1992).
[14]H.-B. Schüttler, J. Zhong, and A. J. Fedro (unpublished).
[15]G. Fano, F. Ortolani, and A. Parola, Phys. Rev. B **46**, 1048 (1992).
[16]W. Stephan and P. Horsch, Phys. Rev. Lett. **66**, 2258 (1991).
[17]E. Dagotto, F. Ortolani, and D. Scalapino, Phys. Rev. B **46**, 3183 (1992).
[18]R. Eder and P. Wróbel, Phys. Rev. B **47**, 6010 (1993); R. Eder, *ibid.* **48**, 13 151 (1993).
[19]Y. Ohta, K. Tsutsui, W. Koshibae, T. Shimozato, and S. Maekawa, Phys. Rev. B **46**, 14 022 (1992).
[20]Y. Ohta, K. Tsutsui, W. Koshibae, and S. Maekawa, Physica B **186-188**, 928 (1993); S. Maekawa, Y. Ohta, and K. Tsutsui, J. Phys. Chem. Solids **54**, 1085 (1993).
[21]See, for example, E. Dagotto and A. Moreo, Phys. Rev. Lett. **63**, 2148 (1989).
[22]Magnetite, Fe_3O_4, may be a possible example. A. Fujimori (private communication); E. J. W. Verwey and P. W. Haaymann, Physica **8**, 979 (1941); E. J. W. Verwey, P. W. Haaymann, and F. C. Romeijn, J. Chem. Phys. **15**, 181 (1947).
[23]P. W. Anderson, Phys. Rev. **102**, 1008 (1956).
[24]J. M. Luttinger, Phys. Rev. **121**, 942 (1961).

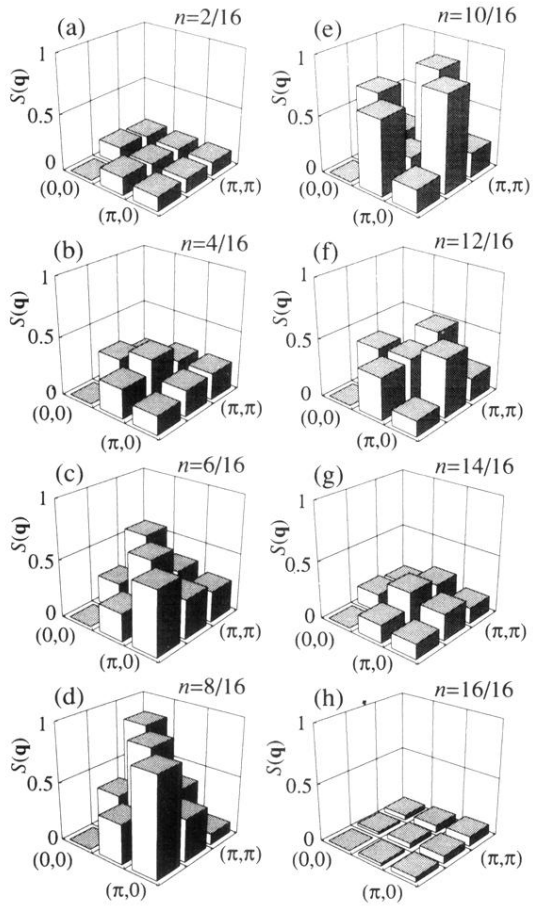

FIG. 2. Filling dependence of the spin correlation function $S(\mathbf{q})$ calculated for the 4×4 cluster with $U/t=8$ and $V/t=3$. The height of the square bar at each $\mathbf{q}$ point indicates the values of $S(\mathbf{q})$. The part of the Brillouin zone with $q_x \geq 0$ and $q_y \geq 0$ is shown.

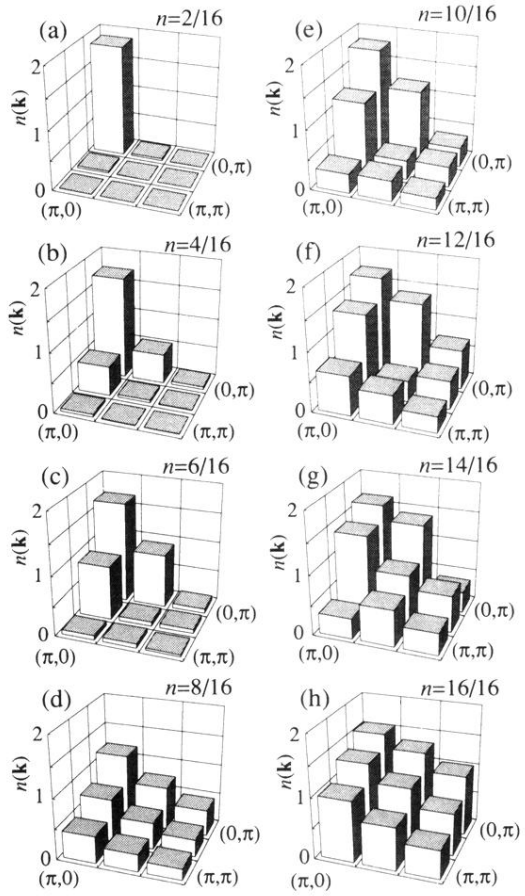

FIG. 8. Momentum distribution function $n(\mathbf{k})$ in the 2D extended Hubbard model calculated for the 4×4 cluster with $U/t=8$ and $V/t=3$. Height of the square bar at each $\mathbf{k}$ point indicates the value of $n(\mathbf{k})$. The part of the Brillouin zone with $q_x \geq 0$ and $q_y \geq 0$ is shown.